

Edge/basal/defect ratios in graphite and their influence on the thermal stability of lithium ion batteries

Carl Erik Lie Foss ^{a,*}, Ann Mari Svensson ^a, Svein Sunde ^a, and Fride Vullum-Bruer ^a
^aDepartment of Material Science and Engineering, Norwegian University of Science and Technology, N-7491 Trondheim, NORWAY

Abstract

Raw graphite can be processed industrially in large quanta but for the graphite to be useful in lithium ion batteries (LIB's) certain parameters needs to be optimized. Some key parameters are graphite morphology, active surface area, and particle size. These parameters can to some extent be manipulated by surface coatings, milling processes and heat treatment in various atmospheres. Industrial graphite materials have been investigated for use as anode material in LIB's and compared with commercial graphite. These materials have been exposed to two different milling processes, and some of these materials were further heat treated in nitrogen atmosphere above 2650 °C. BET combined with density functional theory (DFT) has been employed to study the ratio of basal to non-basal plane and to determine the relative amount of defects. Thermal properties have been investigated with differential scanning calorimetry (DSC). High ethylene carbonate (EC) content improved the thermal stability for graphite with high amount of edge/defect surface area, but showed no improvement of graphite with lower amount of edge/defects. High irreversible capacity loss (ICL) combined with low surface area improved the thermal properties. DFT combined with ICL could potentially be used as a tool to predict thermal stability.

Keywords; lithium ion battery, graphite, thermal stability, DSC, DFT

*Corresponding author

Carl Erik Lie Foss

Email: carl.foss @material.ntnu.no

Phone: +47 97661159

Adress: Valgrindveien 22, 7031 Trondheim, Norway

Introduction

Lithium ion batteries (LIB) have been used commercially since the early 90's when Sony bought the Goodenough patent on LiCoO_2 [1] and used it to make LiCoO_2 /hard carbon batteries. The choice of using lithium ion batteries is mainly due to its high energy density (low weight and high energy). Lithium-ion batteries is therefore the energy storage technology of choice for use in electric vehicles (EV), and it's utilization in other large-scale applications is increasing, like stationary energy storage from renewable sources (wind and PV panels), and ships. These large-scale applications poses new challenges with regards to safety, cycle life and operating conditions. In particular thermal stability is a critical issue for application of lithium-ion batteries in road vehicles and maritime applications.

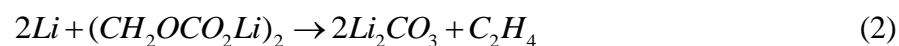
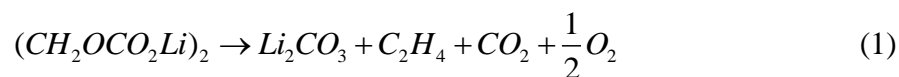
Graphite has been the main choice as anode material in lithium ion batteries because of its availability, stability, capacity and low cost. The electrolytes most commonly used have been the combination of cyclic carbonates, like ethylene carbonate (EC) and propylene carbonate (PC), together with linear carbonates, like diethylene carbonate (DEC), dimethyl carbonate (DMC), and ethyl methyl carbonate (EMC). However, as the intercalation potential is outside the electrochemical stability window for all known electrolytes, there is an irreversible capacity loss (ICL) during the first cycle due to the reduction of electrolyte species. After the reduction, a passive film is formed, preventing further reduction and increasing the stability of the graphite/electrolyte interface. This film is commonly termed the solid electrolyte interphase (SEI) [2]. Prior to this film formation, solvent species could co-intercalate into the graphite structure, causing exfoliation [3], but for electrolytes containing EC (and not PC), severe exfoliation is prevented.

The reduction product of EC, lithium ethylene dicarbonate ($\text{CH}_2\text{OCO}_2\text{Li}$)₂, (referred to as LEDC), and Li_2CO_3 are among the best passivating species due to their small size and polar nature[4]. EC is therefore known to be a vital electrolyte component when it comes to the formation of the SEI. The composition of the SEI has been reported to be a complex mixture of compounds, which in addition to EC reduction products may contain $\text{CH}_3\text{OCO}_2\text{Li}$ (Lithium Methyl Carbonate, LMC), $\text{CH}_3\text{CH}_2\text{OCO}_2\text{Li}$ (lithium ethyl carbonate, LEC), Li_2CO_3 , Li_2O , LiF , and $\text{Li}_x\text{PF}_y\text{O}_z$ [ref: Verma, P.; Maire, P.; Novak, P., *Electrochim. Acta*, 2010, 55, 6332]. It has also been established that the composition of the SEI depends on the surface structure of the graphite, as the edge planes, through which lithium intercalates [11-13], are rich in salt reduction products, whereas the basal planes are dominated by the solvent reduction products (ref: Peled et al, *Electrochimica Acta*, 2004, 391-395). Lithium will only intercalate through

The surface properties of the graphite, both total BET surface area and the total amount of active surface area (ASA), have proven to be important parameters with regards to the first cycle irreversible capacity loss (ICL) [5, 6], as well as formation of a stable and conductive SEI layer. However, a more recent study by Placke et.al [7] implemented the use of density functional theory (DFT) [8, 9] for the evaluation of nitrogen adsorption data, allowing for the determination of the ratio of non-basal planes (edge/defects) vs. basal planes of the surface of the graphite. In their study, variations in the the amounts of defects with heat treatment of the graphite in oxygen atmosphere was studied. Furthermore, upon cycling of the graphite anodes, subject to various heat treatment, a linear correlation between ICL and BET surface area was not obtained, as previously reported [10], but rather a strong correlation between non-basal planes and ICL was found.

On the other hand, a higher percentage of edge planes could be advantageous for cycling at higher charge rates, and an increased amount of edge planes compared to basal planes has been found to reduce the charge transfer resistance [14].

Additionally, the surface properties can have a large effect on the thermal properties. Flaky morphology showed a much earlier onset temperature for exothermic reaction upon heating compared to round particle morphology [15]. This was attributed to an insufficient SEI formation, leaving many sites available for electrolyte reactions. This conclusion was based on the fact that the first exothermic reaction in anode materials for lithium ion batteries is related to the conversion of meta-stable SEI species to more stable species [16], according to Eq. (1-2)



Reaction in Eq. 2 has been suggested to be more likely, as no exothermic peak was observed for de-lithiated samples in the temperature range of 80-120 °C [17]. As it turns out, the state of charge (SOC) (or degree of lithiation) can have a large impact on the thermal response of the anode material, and studies have shown that there is generally a higher thermal response for samples with high state of charge (high concentration of lithium) [16, 18]. Conversion of meta-stable species by ageing at various temperatures also improved the thermal stability (increased the onset temperature for exothermic reactions) [15]. XPS studies of at elevated

temperatures has shown an increase in LiF species (in LiPF₆ containing electrolytes) with storage temperature [19]. In addition, Li₂CO₃ can also be formed according to Eq. (1-2) above [16]. It is clear that the properties of the SEI highly influence the thermal properties of the anode. The SEI is again highly influenced by surface area and structure [5, 6 + 7 + Peled SEI paper] and formation conditions [20] in addition to the electrolyte solvent [21].

The scope of this paper is to investigate the effect of the carbon surface structure on the thermal stability of the cycled anodes. Different graphites, including both commercial battery grade graphites, as well as non-commercial graphites, exposed to different milling processes and heat treatment, were included in the study. The surface structure (relative area of basal, edge and defects) was determined from nitrogen adsorption evaluated by a DFT model. The graphites were evaluated with respect to ICL and changes in thermal stability. It is for example expected that both milling type and varying heat treatment (in N₂ atmosphere) will have an effect on the cell performance. As little is known about the effect of non-basal plane vs. basal plane on thermal stability, and the results will thus give important knowledge regarding the safety of the battery, and how to optimize the graphite anode for with respect to thermal stability.

Experimental

Graphite SLP30 was used as received from TIMCALTM. Graphite Cpreme G8 and P5 were used as received from CPREME. Graphite A2, H2 and A2-2650, H2-2650, supplied by Elkem Carbon, have undergone varying degree of heat treatments (HT). Both A2/H2 and A2-2650/H2-2650 have undergone a graphitization process by heat treatment in N₂ atmosphere between 2300-3000 °C. However, for the A2-2650 and H2-2650 the minimum temperature has been set at 2650 °C, whereas for A2 and H2 the minimum temperature was set to 2300 °C. The difference between A2 and H2 is mainly the milling method. The A-samples were grinded by use of an Alpine mill (jet milling) while H samples were grinded by use of a Hicom mill (high –intensity tumbling mill).

The graphite electrodes were prepared by tape casting slurries consisting of 37 g active graphite material (SLP30/G8/P5/A2/H2), 2 g PVDF (Kynar, reagent grade), 1 g Super P (TIMCALTM), and 60 g 1-methyl-2-Pyrrolidinone (Sigma-Aldrich > 99.5%) onto a 10 µm thick Cu-foil current collector from Circuit foil Luxembourg. The tape caster was a “K Control Coater” from Printcoat instruments. The casts were dried in a vacuum oven at 120 °C overnight.

The electrolytes were made using 4:3:3 or 1:2:2 weight ratio of ethylene carbonate (Sigma-Aldrich > 99 %), ethyl methyl carbonate (Merck, > 99 %), and dimethyl carbonate (Sigma-Aldrich, > 99 %). All solutions are with 0.9 M LiPF₆ (Aldrich, >99.99 %) electrolyte salt unless otherwise specified.

The electrochemical measurements were performed with coin cells from Hohsen Corp which were assembled and sealed inside an argon-filled glove box (O_2 and $H_2O < 0.1$ ppm). The cells consisted of a graphite working electrode (2.01 cm^2) with a loading of about 3 mg/cm^2 , separator (Celgard® 2320), and 0.75 mm thick lithium foil (1.54 cm^2) as counter electrode. All potentials are reported vs. Li/Li^+ unless otherwise specified. The cells were initially charged with a model 4200 potentiostat from Maccor at constant current of 10 mA/g until 5 mV vs. Li/Li^+ , followed by a constant current of 5 mA/g until the current dropped to 5 mA/g to ensure the graphite was fully lithiated. The cells were then discharged with constant current of 10 mA/g until 1.5 V . The subsequent cycles were performed between 0.005 and 1.5 V at the given rate. All experiments were performed at room temperature ($18\text{-}24\text{ }^\circ\text{C}$) unless otherwise specified.

Nitrogen adsorption data was recorded with Tristar 3020 from Micromeritics to obtain the BET surface area (in m^2/g) and DFT surface area, including the deconvolution into basal, edge and defect surfaces. The evaluation of the adsorption data based on the DFT model is embedded in the software from Micromeritics, and follow the theory by Ross and Olivier [8, 9].

Scanning electron microscopy (SEM) was performed with a Hitachi S-3400N in secondary electron mode.

Differential scanning calorimetry (DSC) measurements were performed using a DSC PerkinElmer DSC 7. The temperature range for the high temperature measurements was from 30 to $300\text{ }^\circ\text{C}$ with $2.5\text{ }^\circ\text{C}/\text{min}$ heating rate. 3 samples of 5 mm diameter were cut out from fully lithiated graphite electrodes (after 60 cycles) and placed in gold plated stainless steel

high pressure capsules (from PerkinElmer), together with 3 μl of the same electrolyte used in that specific battery system, and completely sealed inside an argon-filled glove box (O_2 and $\text{H}_2\text{O} < 0.1$ ppm).

Results and discussion

Fig. 1 shows the incremental surface areas vs. adsorptive potential as obtained by the DFT analysis, of graphites A2, H2 (with and without extended heat treatment as explained in the experimental section). These figures show how Nitrogen is adsorbed at different energies depending on the surface of the graphite. The adsorption energies centered around 50-60 K are generally attributed to the basal planes [8, 22]. Adsorption energies below 50 K are related to the edge/prismatic planes, while those above 60 K are related to defects. There is a response emerging at very low adsorption potentials for the heat treated samples, while the relative amount of defects is more or less unchanged. Adsorption potentials are generally determined by the difference in the density of adsorbent constituent atoms at the interface [8]. Extended heat treatment therefore seems to decrease the density of carbons at certain sites, which would explain the peak emerging at lower adsorptive potentials (Fig. 1b and 1d).

BET and DFT surface areas and ICL values for the graphites used in this study are summarized in Table 1. The BET and the DFT surface areas are quite similar, although DFT surface areas give slightly higher values for all the materials. This difference in BET and DFT is consistent with previous studies, and is related to the different assumptions made in the evaluation of data [7]. These are mainly that the BET method assumes a homogeneous surface, while the DFT method assumes a heterogeneous surface [23]. DFT surface area clearly indicate that the amount of edge planes decreased upon extended heat treatment at the expense of basal planes for both A2 and H2. Results further show that both the total surface area and edge/defect surface area decreases upon heat treatment, which consequently decreased the ICL. No significant differences in the amount of defects are observed.

One of the main observations from the data in Table 1 is that the ICL seems to increase with both increasing total surface area (Fig. 2a) and fraction of “non-basal” (edge/defect) planes (Fig. 2b). There is in fact a linear response (except for G8 which shows some deviation from linearity) showing a correlation between a larger surface area and an increase in the ICL.

Fig. 3 shows cumulative pore volume as a function of pore size. It can be seen that the pore volume due to micropores as emerging from the DFT data is basically negligible, and cumulative pore volume is not significant for pores of diameter well below 2 nm. The pore volume is decreased upon extended heat treatment, which can be expected due to grain growth and Ostwald ripening. However, none of the graphites investigated here showed any pores in the micropore area (below 2 nm). This indicates that the Li-electrolyte complexes are able to access all of the active surface area upon wetting and should be able to intercalate through exposed edge planes and defect sites [24].

SEM images of the graphites utilized in this study (Fig. 4), illustrates the difference in morphology. In general, the commercial graphites, SLP30, P5 and G8 exhibits a rounder shape compared to the raw industrial graphites (A2/H2), which are flakier. The commercial materials have most likely been subject to surface treatments (coating and/or spheroidization) This is probably the main reason why A2 and H2 show significantly higher BET surface area compared to the commercial materials.

[evt. Legge inn nye Raman eller XRD her – legg merke til at Placke et al også har gjort Raman, og finner en svak korrelasjon med DFT data]

Fig. 5 shows the thermal response of fully lithiated SLP30, P5 and A2-2650 in 1:2:2 EC:DMC:EMC electrolyte. Notably, the overall heat evolved increases with increasing surface area; A2-2650 > SLP30 > P5. This is reasonable as a larger surface area would cause more SEI to be formed (higher ICL), and the SEI is known to be responsible for the exothermic reactions in the temperature range from 60-230/240 °C [reference would be appropriate, for example ref 17, Haik et al]. However, there is a slightly lower onset peak temperature of the first exothermic reaction in P5 (around 101 °C) compared to SLP30 (around 108 °C).

To further investigate the effect of surface area on the onset peak temperature for the first exothermic reactions, graphite G8 was studied as well (Fig. 6). The inset in shows a magnified view of the first exothermic reactions and, as is observed, there is a clear trend with increased onset peak temperature for the first exothermic reaction with increasing surface area: SLP30 (6.16 m²/g and onset peak temperature around 108 °C) > P5 (3.48 m²/g and onset peak temperature around 101 °C) > G8 (1.79 m²/g and onset peak temperature around 98 °C).

It is possible that the ratio of basal to non-basal plane is the main reason for this difference in onset temperature due to the fact that both thickness and composition of the SEI is expected to be different on basal planes compared to edge planes and defects. However as both total BET surface area and edge/defect surface increase linearly with ICL, it is the total amount of lithium trapped in the SEI compared to the total active surface area that is the main contributing factor influencing thermal behavior. The higher ICL to total surface area ratio of G8 is very likely the reason why G8 has such a low peak in the initial exothermic reaction, and slightly higher heat evolution compared to P5 (which has a higher surface area) at higher temperatures. One could argue that G8 in fact exhibits the better properties in terms of

thermal stability, since even though the actual onset temperature is similar to P5 and the heat evolved is higher compared to P5, the overall heat evolved is delayed to the higher temperatures due to the very dense and protective SEI film (as indicated by a high ICL to surface area ratio). SEM micrographs show that all three materials have similar morphology (Fig. 4), and it is therefore reasonable to believe that it is the amount of surface area and not the shape of the surface which is the main factor to consider in terms of thermal stability. However, it should be noted that Cpreme coats their graphite with a uniform homogenous "graphite-on-graphite" coating to reduce surface area, reducing the overall heat evolution, and thereby improving safety [ref?]. It is suspected that TIMCALTM also coats their graphite SLP30 due to their smooth potato shaped morphology. If all these commercial graphites are coated it would most likely influence their thermal properties, particularly since it is uncertain whether the coating is amorphous or crystalline. It is worth mentioning that the A2/H2 graphites are un-coated and that their morphology is flakier with a less smooth surface, which results in a larger surface area compared to the commercial materials. This is also evident from the larger thermal response of graphite A2-2650.

Fig. 7 shows the thermal response of SLP30, P5 and G8 in 4:3:3 EC:DMC:EMC electrolyte. Both P5 and G8 exhibit similar thermal behavior and an onset peak temperature around 100 °C for the first exothermic reaction, which is comparable to what was observed with the electrolyte 1:2:2 EC:DMC:EMC (Fig. 5-6). However, SLP30 shows an onset temperature which is considerably higher in 4:3:3 EC:DMC:EMC compared to 1:2:2 EC:DMC:EMC. Fig. 8 shows a direct comparison between these two electrolytes. Notably a higher EC- content increases the thermal stability for SLP30, but not for G8 and P5. One possibility is that SLP30 requires a higher amount of EC for stable SEI formation due to larger edge/defect surface area compared to P5/G8 (edge/defect surface area is the most active surface towards

EC reduction). For SLP30 the electrolyte with 40 % EC showed a higher onset temperature for the first exothermic reaction compared to the electrolyte with 20 % EC, while the latter exhibited higher heat evolution in the temperature range from 120-240 °C.

The higher heat evolution can be attributed to the fact that the system with 20 % EC probably has a less compact (more porous) SEI, since it is mainly the decomposition product of EC ($(\text{CH}_2\text{OCO}_2\text{Li})_2$ and Li_2CO_3 , which are regarded as the species responsible for providing a compact and passivating SEI [25]. This would allow for easier diffusion of lithium from the graphite structure to the surface, consequently causing reactions with the electrolyte to form stable species (like LiF and Li_2CO_3). This occurs until all sites are blocked [18], leading to a structural collapse around 240 °C, which would account for the endothermic peak (exfoliation). The remaining lithium inside the graphite structure is now allowed to react further, as well as the PVDF (which accounts for the last exothermic reaction above 250 °C).

The lower onset temperature of the electrolyte with 20 % EC could be explained in the same manner, by a more porous SEI. A more porous structure would, as mentioned, allow for easier reaction between intercalated lithium and the electrolyte. In the electrolyte with 40 % EC, the SEI is expected to consist of very stable passivating species and is probably more compact. There are most likely fewer sites available for reaction between intercalated lithium and the electrolyte. It is therefore reasonable that the exothermic reactions occur at higher temperatures.

Conclusion

The total heat evolution of cycled graphitized electrodes together with the relevant electrolyte, as determined by DSC show a clear correlation with the total amount of surface area and thus also the ICL.

However, commercial graphite with low surface area (G8 and P5) showed a lower onset temperature for exothermic reactions (related to conversion of meta-stable species in the SEI to more stable compounds) compared to commercial graphite with larger surface area (SLP30).

Higher relative EC content in the electrolyte led to a higher onset temperature (better thermal stability) for exothermic reactions compared to lower EC content for SLP30. This was attributed to the less stable and more porous SEI formed with low contents of EC, as EC reduction products are required to form a stable SEI. With a more porous morphology, the layer is more exposed to electrolyte, which leads to onset the exothermal reactions.

Thus, there is likely a correlation between a more stable SEI (consisting of stable species like Li_2CO_3 and $(\text{CH}_2\text{OCO}_2\text{Li})_2$) and the onset temperature. Graphites with high amounts of edge planes require more EC to ensure good SEI formation and consequently better thermal properties.

Heat treatment of industrial graphite reduced the overall surface area and caused a decrease in total pore volume and BET surface area, as verified by nitrogen adsorption experiments.

There seem to be a trend that ICL, amount edge/defect, and amount of EC (all related to formation of stable SEI), can influence the thermal stability. High ICL and low edge/defects area are indicative of a stable SEI with good thermal properties. One of the main conclusions

from the data presented here is that relative amounts of surface sites, coupled with ICL data, could be a potentially useful tool to predict thermal stability behavior of graphites in Li-ion batteries. In addition they can be used to tailor the amount of EC needed to form a protective film with good thermal properties for any given graphite material.

Acknowledgments

The Norwegian Research Council (grant number 195432/S10), SINTEF, and NTNU. The industrial partners, Elkem Carbon AS, Miljøbil Grenland AS and Carbontech Holding AS are acknowledged for their co-funding of the project.

References

1. K. Mizushima, et al., *LixCoO₂ (0 < x < 1): A new cathode material for batteries of high energy density*. Materials Research Bulletin, 1980. **15**(6): p. 783-789.
2. E. Peled, *The Electrochemical-Behaviour of Alkali and Alkaline-Earth Metals in Non-Aqueous Battery Systems - The Solid Electrolyte Interphase Model*. Journal of the Electrochemical Society, 1979. **126**(12): p. 2047-2051.
3. J.O. Besenhard, et al., *Filming mechanism of lithium-carbon anodes in organic and inorganic electrolytes*. Journal of power sources, 1995. **54**(2): p. 228-231.
4. D. Aurbach, et al., *On the correlation between surface chemistry and performance of graphite negative electrodes for Li ion batteries*. Electrochimica Acta, 1999. **45**(1): p. 67-86.
5. S.H. Ng, et al., *Correlations between surface properties of graphite and the first cycle specific charge loss in lithium-ion batteries*. Carbon, 2009. **47**(3): p. 705-712.
6. P. Novák, et al., *The importance of the active surface area of graphite materials in the first lithium intercalation*. Journal of power sources, 2007. **174**(2): p. 1082-1085.
7. T. Placke, et al., *Influence of graphite surface modifications on the ratio of basal plane to non-basal plane surface area and on the anode performance in lithium ion batteries*. Journal of power sources, 2011. **200**(0): p. 83-91.
8. J.P. Olivier and M. Winter, *Determination of the absolute and relative extents of basal plane surface area and "non-basal plane surface" area of graphites and their impact on anode performance in lithium ion batteries*. Journal of power sources, 2001. **97-98**: p. 151-155.

9. J.P. Olivier and S. Ross, *On Physical Adsorption. XVI. The Physical Interaction of H₂, D₂, CH₄, and CD₄ with Graphite*. Proceedings of the Royal Society of London. Series A. Mathematical and Physical Sciences, 1962. **265**(1323): p. 447-454.
10. F. Joho, et al., *Relation between surface properties, pore structure and first-cycle charge loss of graphite as negative electrode in lithium-ion batteries*. Journal of power sources, 2001. **97-98**: p. 78-82.
11. T. Tran and K. Kinoshita, *Lithium intercalation deintercalation behaviour of basal and edge planes of highly oriented pyrolytic-graphite and graphite powder*. Journal of Electroanalytical Chemistry, 1995. **386**(1-2): p. 221-224.
12. Y. NuLi, J. Yang, and Z. Jiang, *Intercalation of lithium ions into bulk and powder highly oriented pyrolytic graphite*. Journal of Physics and Chemistry of Solids, 2006. **67**(4): p. 882-886.
13. A. Funabiki, M. Inaba, and Z. Ogumi, *A.c. impedance analysis of electrochemical lithium intercalation into highly oriented pyrolytic graphite*. Journal of power sources, 1997. **68**(2): p. 227-231.
14. Y. Yamada, K. Miyazaki, and T. Abe, *Role of Edge Orientation in Kinetics of Electrochemical Intercalation of Lithium-Ion at Graphite*. Langmuir. **26**(18): p. 14990-14994.
15. E.P. Roth and D.H. Doughty, *Thermal abuse performance of high-power 18650 Li-ion cells*. Journal of power sources, 2004. **128**(2): p. 308-318.
16. M.N. Richard and J.R. Dahn, *Accelerating rate calorimetry study on the thermal stability of lithium intercalated graphite in electrolyte I. Experimental*. Journal of the Electrochemical Society, 1999. **146**(6): p. 2068-2077.
17. O. Haik, et al., *On the Thermal Behavior of Lithium Intercalated Graphites*. Journal of the Electrochemical Society, 2011. **158**(8): p. A913-A923.

18. H. Yang, et al., *Investigations of the exothermic reactions of natural graphite anode for Li-ion batteries during thermal runaway*. Journal of the Electrochemical Society, 2005. **152**(1): p. A73-A79.
19. A.M. Andersson and K. Edstrom, *Chemical Composition and Morphology of the Elevated Temperature SEI on Graphite*. Journal of the Electrochemical Society, 2001. **148**(10): p. A1100-A1109.
20. S.S. Zhang, K. Xu, and T.R. Jow, *Optimization of the forming conditions of the solid-state interface in the Li-ion batteries*. Journal of power sources, 2004. **130**(1-2): p. 281-285.
21. K. Kanamura, et al., *Morphology and chemical-compositions of surface-films of lithium deposited on a Ni substrate in nonaqueous electrolytes*. Journal of Electroanalytical Chemistry, 1995. **394**(1-2): p. 49-62.
22. J. Olivier, Adsorption of carbons, 2008: p. CH7.
23. J. Olivier and M. Winter, *Determination of the absolute and relative extents of basal plane surface area and "non-basal plane surface" area of graphites and their impact on anode performance in lithium ion batteries*. Journal of power sources, 2001. **97-8**: p. 151-155.
24. H.T. Zhou, M.A. Einarsrud, and F. Vullum-Bruer, *High capacity nanostructured Li₂Fe_xSiO₄/C with Fe hyperstoichiometry for Li-ion batteries*. Journal of power sources. **235**: p. 234-242.
25. D. Aurbach, et al., *New insights into the interactions between electrode materials and electrolyte solutions for advanced nonaqueous batteries*. Journal of power sources, 1999. **81**: p. 95-111.

26. F. Joho, P. Novak, and M.E. Spahr, *Safety aspects of graphite negative electrode materials for lithium-ion batteries*. Journal of the Electrochemical Society, 2002. **149**(8): p. A1020-A1024.

Figure 1. Incremental surface area as evaluated by a DFT analysis of nitrogen adsorption data for graphite SLP30. a) A2 b) A2-2650 c) H2 d) H2-2650

Figure 2. Irreversible capacity loss (ICL) vs. a) BET and b) Edge/defect (non-basal) surface area for different graphite samples in 1:2:2 EC:DMC:EMC + 0.9M LiPF₆ electrolyte.

Figure 3. Cumulative volume vs. pore diameter for different graphite samples.

Figure 4. SEM images of graphite a) A2, b) A2-2650, c) H2, d) H2-2650, e) G8, f) P5 and g) SLP30.

Figure 5. Differential scanning calorimetry for fully lithiated graphites (SLP30, P5 and A2-2650) after 60 cycles in 1:2:2 EC:DMC:EMC + 0.9M LiPF₆ electrolyte. The heating rate was 2.5 °C/min.

Figure 6. Differential scanning calorimetry for fully lithiated graphites (SLP30, P5 and G8) after 60 cycles in 1:2:2 EC:DMC:EMC + 0.9M LiPF₆ electrolyte. The heating rate was 2.5 °C/min. Inset shows a magnified view of the initial exothermic reaction.

Figure 7. Differential scanning calorimetry for fully lithiated graphites (SLP30, P5 and G8) after 60 cycles in 4:3:3 EC:DMC:EMC + 0.9M LiPF₆ electrolyte. The heating rate was 2.5 °C/min.

Figure 8. Differential scanning calorimetry for fully lithiated graphites SLP30 after 60 cycles in 1:2:2 EC:DMC:EMC + 0.9M LiPF₆ and 4:3:3 EC:DMC:EMC + 0.9M LiPF₆ electrolyte. The heating rate was 2.5 °C/min.